

Simulation of Small Radio Telescope Antenna Parameters at Frequency of 1.42 GHz

Uday E. Jallod^{a1*}, Hareth S. Mahdi^{b1}, and Kamal M. Abood^{c1}

¹Department of Astronomy and Space, College of Science, University of Baghdad, Baghdad, Iraq

^bE-mail: hareth@uobaghdad.edu.iq, ^cE-mail: kamal.abood@sc.uobaghdad.edu.iq

^{a*}Corresponding author: uday.jallod@sc.uobaghdad.edu.iq

Abstract

The paper presents an overview of theoretical aspects of small radio telescope antenna parameters. The basic parameters include antenna beamwidth, antenna gain, aperture efficiency, and antenna temperature. These parameters should be carefully studied since they have vital effects on astronomical radio observations. The simulations of antenna parameters were carried out to assess the capability and the efficiency of small radio telescopes to observe a point source at a specific frequency. Two-dimensional numerical simulations of a uniform circular aperture antenna are implemented at different radii. The small diameter values are chosen to be varied between (1-10) m. This study focuses on a small radio telescope with a diameter of 3 m since this telescope is very common in the world. The simulated results of this study illustrated that the power pattern of a 3 m antenna has a half-power beamwidth of approximately 5 degrees. Also, the maximum peak antenna temperature is estimated to be more than 3000 K. All of these results were in good agreement with observations of the neutral hydrogen spectral line at the frequency of 1.42 GHz using a small radio telescope.

Article Info.

Keywords:

Antenna, radio telescope, circular aperture, power pattern, antenna temperature.

Article history:

Received: Oct. 13, 2021

Accepted: Jan. 20, 2022

Published: Mar. 01, 2022

1. Introduction

Antennas are part of a transmitting or a receiving system that is designed to radiate or receive an electromagnetic wave. There are many types of antennas according to radiating or receiving the electromagnetic fields [1]. Different antennas are suited for operation at different frequencies and could be categorized into four groups with varying modes of operation; current elements, traveling wave, array, and aperture [2]. In an aperture antenna, the radiated electromagnetic fields should possess their maximum value in the direction of the main lobe while possessing a minimum value in the direction of the side and back lobes. For this reason, a sensitivity of a radio telescope is increased; therefore, a large number of aperture antennas are used, including reflectors, lenses, and horn antennas [3]. There are many different geometrical configurations of an aperture antenna; they may take the form of a waveguide or horn whose aperture may be square, rectangular, elliptical, circular, or any other configuration [4]. A circular aperture antenna with a physical opening with a circular shape is used at microwave and millimeter-wave frequencies and is usually operated in wavelength less than about 0.3 m [1].

Several circular aperture antennas are encountered in practice, especially in radio astronomy and space applications.

While designing a radio telescope antenna, various parameters need to be considered. These parameters such as bandwidth, gain, directivity, beam width, and radiation pattern characterize an antenna's performance [5]. The radiation pattern is the essential parameter of antennas that allows designers to compare different solutions and assess their usefulness in wireless communication systems. The radiation pattern of the circular aperture antenna is determined by the value of the aperture diameter and current distribution function on the aperture. This antenna radiation pattern may be illuminated uniformly or non-uniformly distributed on the reflector dish [6]. The power pattern of a uniformly illuminated circular aperture is the airy disk pattern. This pattern behaves as a function of wavelength and aperture size. If the aperture field distribution amplitude is constant, this is referred to as uniform aperture, while if the field distribution amplitude is tapered from the center toward the edge of the aperture, this is called grading or tapered circular aperture [7].

To solve the far-field antenna radiation pattern, various methods have been developed. The methods are based on the equivalence principles of physical optics. Modern analysis techniques are built up by replacing the physical aperture antenna with a virtual aperture. Two techniques could be used conveniently to account for the edge aperture effects. One technique is the Method of Moments (MOM), and the other is the Geometrical Theory of Diffraction (GTD) which Keller originally developed in the 1950s [8]. The MOM describes the solution as an integral and could be used to handle arbitrary shapes [9]. GTD, on the other hand, is an extension of classical Geometrical Optics (GO), and it is used to overcome some of the limitations of GO by introducing a diffraction mechanism [10]. An incoming incident rays striking an edge surface boundary creates a non-uniform diffracted beam. GTD technique is used to describe the diffraction at a particular region called the shadow, wherein the electric field is assumed to be zero for the ordinary GO [11].

Two types of mathematical formulation are available for computing the electromagnetic field of waves radiated by the aperture. The first is scalar diffraction, and the second is vector diffraction. The scalar diffraction technique has many practical applications in radio observing systems [12]. There are two approaches of scalar diffraction, which are classified into near and far-field approximation according to the distance between the source and the observation plane. When the distance is infinitely large, it is called far-field approximation; within which the Fraunhofer diffraction pattern occurs. In contrast, if the distance is large but finite, this is called near field approximation and represented by Fresnel diffraction integral [13].

In our study, the mathematical equations that compute antenna power patterns have been studied and simulated to demonstrate small radio telescopes' essential features. Two-dimensional computer simulations of a uniform circular aperture antenna were implemented at different radii. These simulations were carried out to study antenna parameters: antenna beam width, antenna gain, aperture efficiency, and antenna temperature.

2. Theoretical considerations

The radiation pattern can be expressed in terms of electric field intensity. At a far-field distance from the antenna, it is convenient to denote the field by spherical coordinate components: elevation (θ) and azimuth (ϕ). Then the pattern depends on two variables only since the distance is constant, which greatly simplifies the matter

[14]. The geometry associated with the parabolic antenna's circular aperture is depicted in Fig. 1.

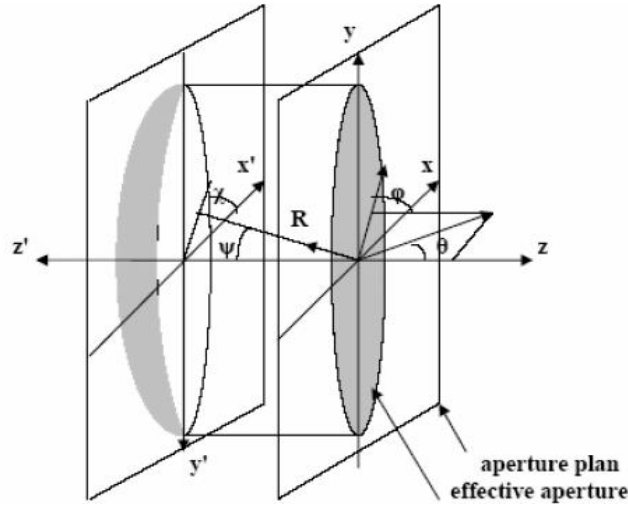


Figure 1: Geometry of parabolic reflector antenna and its projected effective antenna [14].

The diffraction theory provides the relationship between the radiated field $F(x, y)$ and the aperture illumination $f(x', y')$. Then the electric far-field can be given by Fraunhofer diffraction integral [15]:

$$F(x, y) = \frac{1}{2\pi} \iint f(x', y') e^{iks \sin\theta (x' \cos\phi + y' \sin\phi)} dx' dy' \quad (1)$$

where x', y' are the plane dimensions of an observing system, and k is the wavenumber.

The polar coordinate system (ρ, ψ) used to describe a point in an aperture plane and to analyze the radiation of a circular aperture of diameter (D) , where (ρ) is the radial distance of the ray inside the aperture, and (ψ) is the angle of the reflected ray. Therefore, the observing system dimensions could be written in a polar system according to the following formulae [$x' = \rho \cos \psi, y' = \rho \sin \psi$, and $dx' dy' = \rho d\rho d\psi$]. Therefore, Eq. (1) can be rewritten as follows [16]:

$$F(\phi, \theta) = \frac{1}{2\pi} \int_0^{2\pi} \int_0^\infty f(\rho, \psi) e^{ik\rho \sin\theta (\cos\phi \cos\psi + \sin\phi \sin\psi)} \rho d\rho d\psi \quad (2)$$

Furthermore, if it is circularly symmetric, i.e. $f(\rho, \psi) = f(\rho)$, then this leads to the radiated field (F) to be independent on (ϕ) . Therefore, Eq. (2) is reduced to become:

$$F(\theta) = \int_0^\infty \left[\frac{1}{2\pi} \int_0^{2\pi} e^{ik\rho \sin\theta \cos(\phi-\psi)} d\psi \right] f(\rho) \rho d\rho \quad (3)$$

Since, the Bessel function of zero-order $J_0(z)$ is defined as [16]:

$$J_0(z) = \frac{1}{2\pi} \int_0^{2\pi} e^{iz \cos(\phi-\psi)} d\psi \quad (4)$$

Therefore, Eq. (3) can be written as:

$$F(\theta) = \int_0^\infty f(\rho) J_0(k\rho \sin\theta) \rho d\rho \quad (5)$$

the current distribution function can also represent $f(\rho)$ as [17]:

$$f(\rho) = \left[1 - \left(\frac{2\pi\rho}{D} \right)^2 \right]^m$$

where m is an integer value, the distribution type when $m = 0$ refers to a uniform distribution, and the current distribution function is unity.

Consequently, Eq. (5) is reduced to become:

$$F(\theta) = \int_0^\infty J_0(k\rho \sin\theta) \rho d\rho \quad (6)$$

This is also called Hankel transform, the Fourier – Bessel function transform. The normalized power pattern P is given as [17]:

$$P(\theta) = \left[\frac{\int_0^\infty J_0(k\rho \sin\theta) \rho d\rho}{\int_0^\infty \rho d\rho} \right]^2 \tag{7}$$

For Bessel functions, the following property is used to solve Eq. (7) [18]:

$$\int J_0(xr) r dr = \frac{2J_1(x)}{x}$$

Then the normalized power pattern (P) is given by [19]:

$$P(U) = \left[\frac{2J_1\left(\frac{\pi UD}{\lambda}\right)}{\left(\frac{\pi UD}{\lambda}\right)} \right]^2 \tag{8}$$

Eq. (8) is obtained by substituting, $U = \sin \theta$, $k = \frac{2\pi}{\lambda}$, and $\rho \leq \frac{D}{2}$. J_1 is the first order of the Bessel function.

3. Results and discussion

Two-dimensional computer simulations were carried out to investigate the essential features of the antenna power pattern. The uniform circular aperture of the radio telescope was generated in an array of size 128 by 128 pixels according to Eq. (8). Eq. (8) was simulated at a frequency of (1.42 GHz or 0.21 m in wavelength). The dependence of the characteristics of a small radio telescope of different diameters was investigated. To verify our simulations, the antenna diameter was assumed to be (1 m, 2 m, 3 m, 4 m, 5 m, and 10 m). The results are displayed in Fig. 2.

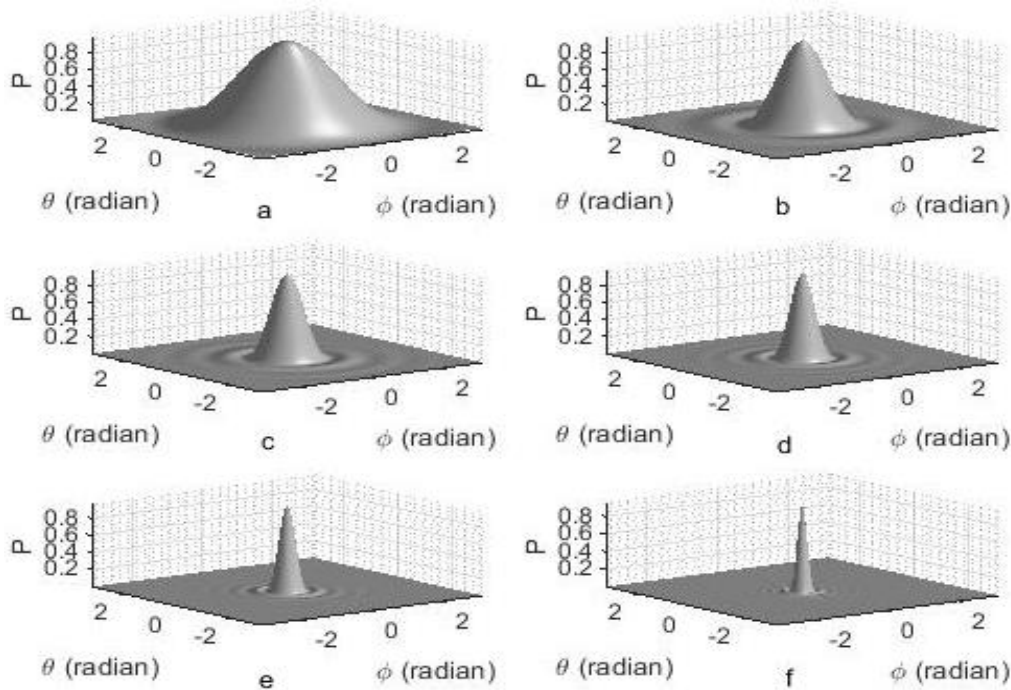


Figure 2: Normalized power pattern (P) as a function of (azimuth (ϕ), elevation (θ)): a – Antenna diameter ($D = 1$ m), b – Antenna diameter ($D = 2$ m), c – Antenna diameter ($D = 3$ m), d – Antenna diameter ($D = 4$ m), e – Antenna diameter ($D = 5$ m), and f – Antenna diameter ($D = 10$ m).

The side lobes are hard to be resolved, as shown in Fig. 2. Because the power pattern (P) of the parabolic reflector antenna was concentrated in the main lobe, therefore, the contributions of these side lobes can be neglected in our observational computations.

The angular width of the main lobe is called beam width. An essential parameter that should be measured with high accuracy is the Half Power Beam width (θ_{HPBW}). θ_{HPBW} is the full width of the normalized power pattern (P) at half power peak. This is equivalent to Rayleigh criterion of resolution and could be written as [20]:

$$\theta_{HPBW} = q \frac{\lambda}{D} \quad (9)$$

q is the beam width factor that depends on the antenna illumination and edge taper usually q varies in different values, like $q = 1$ and $q = 1.2$ [21].

Eq. (9) was used to calculate the θ_{HPBW} for different values of antenna diameter; q and λ are assumed to be 1.2 and 0.21 m, respectively. θ_{HPBW} as a function of antenna diameter is shown in Fig. 3.

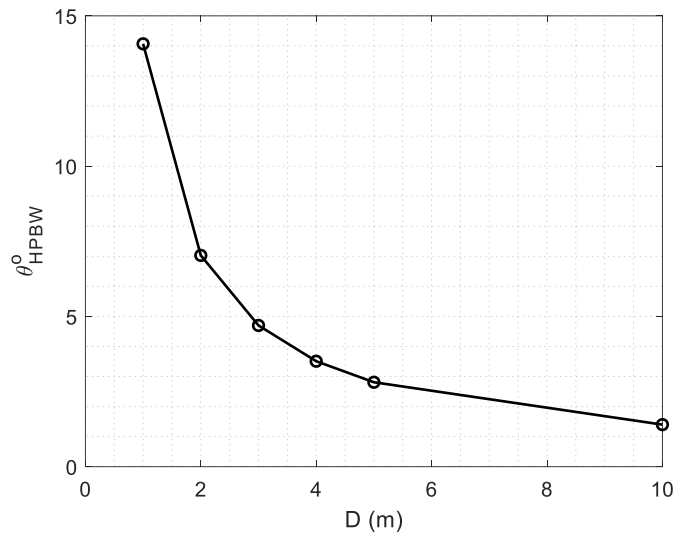


Figure 3: Half Power beam width (θ_{HPBW} (degree)) as a function of the antenna diameter (D (m)).

From Fig. 3, it can be noticed that the angular resolution is inversely proportional to the antenna diameter. This means that a better angular resolution can be obtained when a larger dish is used.

Another helpful measure describing the performance of an antenna is the gain (G). G is considered the antenna's ability to transform the available power at its input terminal to the power pattern (P). This quantity is measured in logarithmic scale in a unit called decibel (dB) and could be computed as follows [22]:

$$G(\text{dB}) = 10 \log_{10}[P(\phi, \theta)] \quad (10)$$

Although the antenna's gain is closely related to the directivity, directivity is a measure that describes only the directional properties of the antenna pattern. G without dissipative losses is equal to its directivity in any given direction. If the direction is not specified, the direction of maximum radiation intensity is implied. G is computed according to Eq. (10), and the result is demonstrated in Fig. 4.

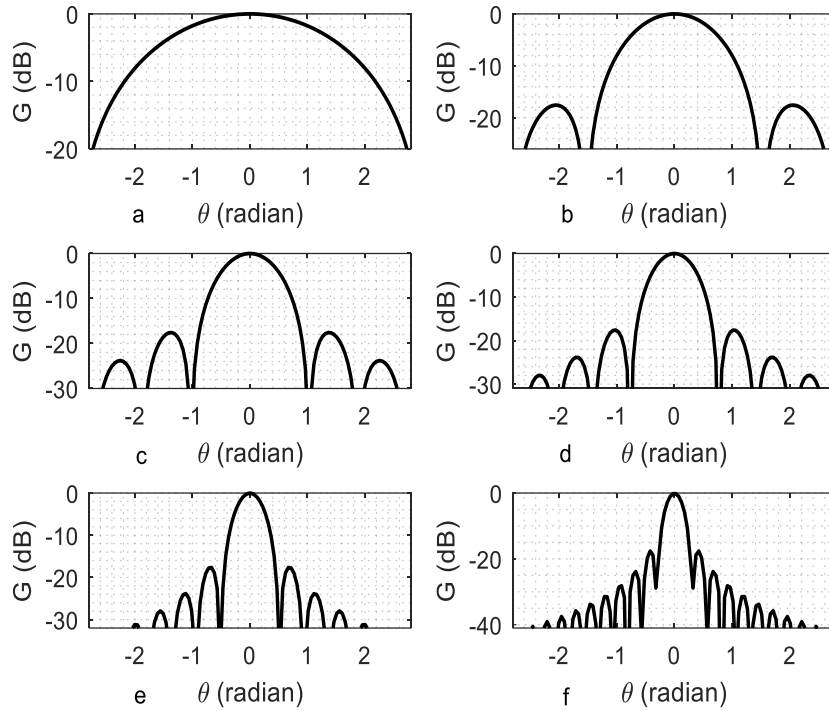


Fig. 4: Antenna gain (G (dB)) as a function of (elevation (θ)): a – Antenna diameter ($D = 1$ m), b – Antenna diameter ($D = 2$ m), c – Antenna diameter ($D = 3$ m), d – Antenna diameter ($D = 4$ m), e – Antenna diameter ($D = 5$ m), and f – Antenna diameter ($D = 10$ m).

The aperture efficiency (η) can be defined as measuring the radiated input powers via an antenna. The common form of (η) is written as [23]:

$$\eta = \frac{A_e}{A_g} \tag{11}$$

where A_e is the effective area and A_g (m^2) can be computed using the following formula [23]:

$$A_g = \frac{\pi D^2}{4} \tag{12}$$

η has been calculated using Eq.s (11 and 12). The result of this computation is demonstrated in Fig. 5.

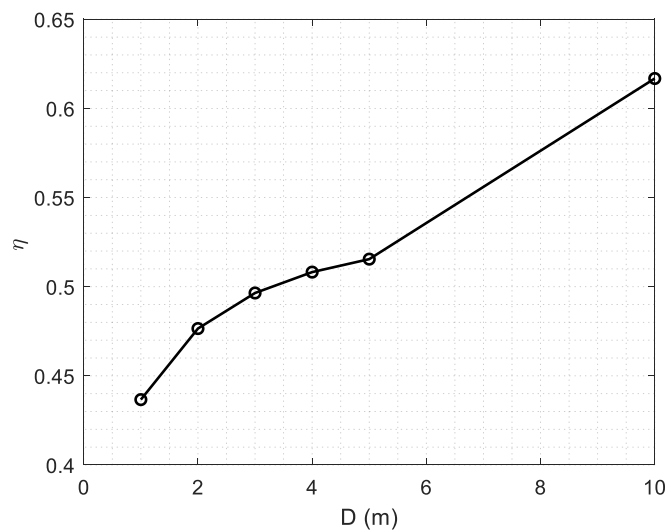


Figure 5: Aperture efficiency (η) as a function of the antenna diameter (D) (m).

Fig. 5 clearly shows that the efficiency increases with the diameter of the antenna. A high efficiency indicates that most of the power fed to the antenna is radiated. In reality, the source intensity measured from a radio telescope can be represented by a Gaussian function as follows [23]:

$$g(x, y) = H e^{-(x+y)^2/2\sigma^2} \tag{13}$$

where (x, y) is the source coordinates, H represents the source intensity, and σ is the standard deviation of the Gaussian function that controls its width.

The fundamental equation that describes the recorded signal by a radio telescope is the antenna power (P_A) equation. This equation is a convolution between the source intensity that is given in Eq. (13) with the normalized power pattern (P), which is given in Eq. (8), and can be given as [24]:

$$P_A(\phi, \theta) = \int_0^{2\pi} \int_0^\pi g(x', y') P(\phi - x', \theta - y') dx' dy' \tag{14}$$

x' and y' are coordinates in an observing system.

The convolution can be computed by taking Fourier transform (FT) for both functions (g and P). Then, this convolution becomes the product of the Fourier transform of the two functions. Since the radio signals are very weak; therefore, H is set to be 10^{-6} . The narrow width (σ) intensity is set to be 0.25. The source intensity is assumed to be weak enough to demonstrate the variations of the recorded signal via the six radio telescopes. Different gain values cause these variations for these radio telescopes. Then, the antenna power (P_A) is computed via the convolution operator. This convolution is applied between the source intensity, which is emitted at 1.42 GHz, and the normalized power patterns (P) of the six radio telescopes, according to Eq. (14). The result is illustrated in Fig. 6.

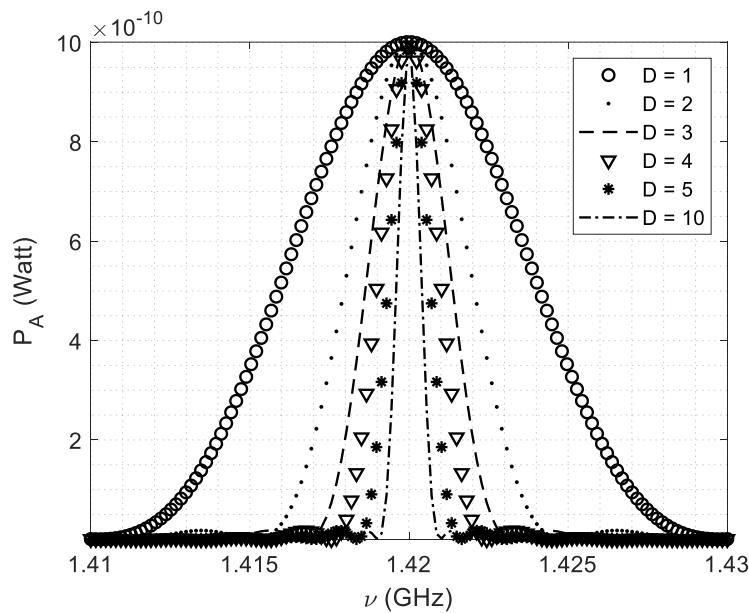


Figure 6: Antenna power (P_A) due to observed the frequency (ν) at different antenna diameters ($D = 1, 2, 3, 4, 5,$ and 10) m.

Fig. 6 indicates that the weak signal reduces the antenna power (P_A) to minimum values. This signal does not fill the antenna power pattern (P). This means that it is independent of the shape of its power pattern.

One antenna characteristic that is difficult to estimate accurately is the antenna temperature (T_A). If the antenna's gain function (G) is known analytically, estimating (T_A) expressions could be extracted. Consequently, it is possible to compute the (T_A) using Nyquist theorem via the relation [24]:

$$T_A = \frac{P_A}{(Gk_B\Delta\nu)} \tag{15}$$

k_B is Boltzmann constant, $\Delta\nu$ receiver frequency bandwidth which was set at (2×10^8 Hz) for the six radio telescopes. The result is shown in Fig. 7.

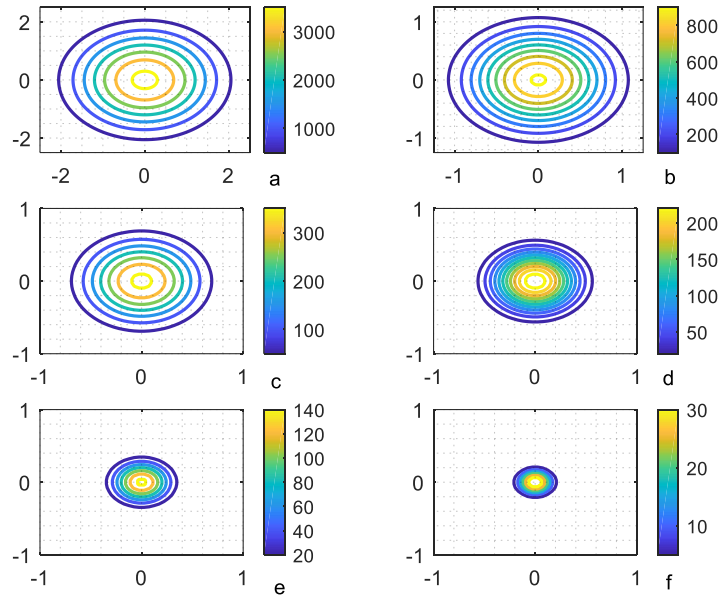


Figure 7: Contour plots of Antenna temperature (T_A) due to observing the frequency ($\nu = 1.42$ GHz), a – Antenna diameter ($D = 1$ m), b – Antenna diameter ($D = 2$ m), c – Antenna diameter ($D = 3$ m), d – Antenna diameter ($D = 4$ m), e – Antenna diameter ($D = 5$ m), and f – Antenna diameter ($D = 10$ m).

The maximum peaks of the antenna temperature (T_A) and its fitting are plotted with the antenna diameter (D) as shown in Fig. 8, T_A decreases exponentially with antenna diameter.

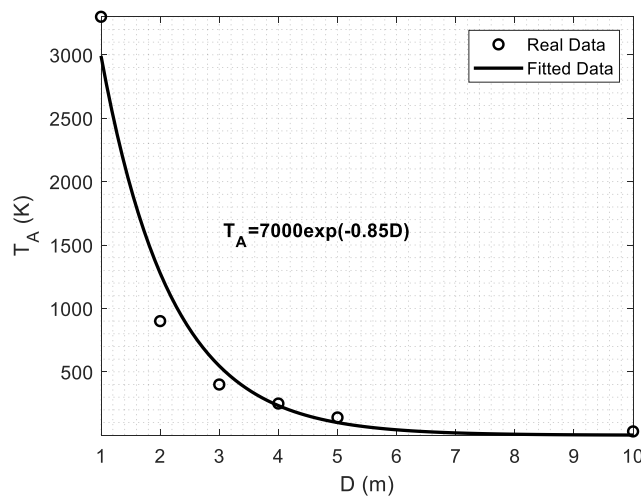


Figure 8: Peaks of antenna temperature (T_A) as a function of the antenna diameter (D (m)).

4. Conclusions

A neutral Hydrogen emission line at the frequency of 1.42 GHz is the major source of radio waves from astronomical objects, and radio telescopes can detect this emission line. In this study, the impact of the characteristics of radio telescopes on their performance and observations was studied. The features investigated in this study were the shape of the power pattern, the Half Power beam width, and antenna gain. The shape of power pattern for a small radio telescope antenna was considered to be a Gaussian illumination pattern since the height of the first side lobe is very small compared to the actual height of the pattern. The Half-Power Beam width (θ_{HPBW}) was estimated at a frequency of 1.42 GHz and found to be 1.2° for a 10 m telescope, 4.8° for a 3 m telescope, and 14° for a 1 m telescope. The antenna gain (dB) has also been estimated and found to be approximately between (20 to 40) dB. The first side level is -17.6 dB; this is considered very low and could be ignored because this level is always blanketed by sky background noise and does not affect observations. Finally, an empirical formula was presented to describe antenna temperature (T_A) and its diameter (D) relationship. This formula is governed by a negative exponential function as given by the equation ($T_A = 7000\exp(-0.85D)$). The result showed that T_A rapidly decreased as approaching $D = 5$ meters and became insignificant afterward. Those results were found to be in good agreement with observational data.

Acknowledgments

The authors would like to express our thanks and gratitude to the head of the Department of Astronomy and Space, academic staff, colleagues, and friends at the College of Science, University of Baghdad, for their valuable advice and encouragement.

Conflict of interest

The authors declare that they have no conflict of interest.

References

1. Balanis C.A., *Antenna theory: analysis and design*. 2015: John Wiley & sons.
2. Jallod U.E., *Calibration of BURT Parameters by using 21 cm Hydrogen Line Emission Observation from the Sun*, Thesis, University of Baghdad, 2020.
3. Rathaur A.S., *Design and simulation of Different Types Antenna using Matlab*. Journal of Science Research Engineering & Technology (IJSRET), 2017. **6**(6): pp. 589-600.
4. Condon J.J. and Ransom S.M., *Essential radio astronomy*. 2016: Princeton University Press.
5. Yeap K.H., Loh M.C., Tham C.Y., Yiam C.Y., Yeong K.C., and Lai K.C., *Analysis of reflector antennas in radio telescopes*. Advanced Electromagnetics, 2016. **5**(3): pp. 32-38.
6. Jankowski-Miñulowicz P., Lichoń W., and Węglarski M., *Numerical model of directional radiation pattern based on primary antenna parameters*. International Journal of Electronics Telecommunications, 2015. **61**(2): pp. 191-197.
7. Leis J.W., *Communication systems principles using MATLAB*. 2018: John Wiley & Sons.
8. Yurduseven O. and Yurduseven O., *Compact parabolic reflector antenna design with cosecant-squared radiation pattern*. Microwaves, Radar and Remote Sensing Symposium, 2011: pp. 382-385.

9. Sandip M. and Anil R., *Computational Electromagnetics: Techniques and Applications*. International Journal for Research in Applied Science & Engineering Technology (IJRASET), 2017. **5**(X1): pp. 121-125.
10. Kildal P.S., *Foundations of antenna engineering: a unified approach for line-of-sight and multipath*. 2015: Artech House.
11. Daly C.J., Nuteson T.W., and Rao N.A., *The spatially averaged electric field in the near field and far field of a circular aperture*. IEEE Transactions on Antennas Propagation, 2003. **51**(4): pp. 700-711.
12. Michael A.O., *On the antenna gain formula*. Int. J. Appl. Sci. Technol, 2013. **3**(1): pp. 43-49.
13. Jallod U.E., *Simulation of Fraunhofer Diffraction for Plane Waves using Different Apertures*. Iraqi Journal of Science, 2015. **56**(2A): pp. 1198-1207.
14. Merabtine N., Boualleg A., and Benslama M., *Analysis of radiation patterns and feed illumination of the reflector antenna using the physical and geometrical optics*. Semiconductor Physics Quantum Electronics Optoelectronics, 2006. **9**(2): pp. 53-57.
15. Marr J.M., Snell R.L., and Kurtz S.E., *Fundamentals of radio astronomy: observational methods*. Vol. 13. 2015: CRC Press.
16. Singh A., Loonker D., and Banerji P., *Fourier-Bessel transform for tempered Boehmians*. Int. Journal of Math. Analysis, 2010. **4**(45): pp. 2199-2210.
17. Rohlfs K. and Wilson T.L., *Tools of radio astronomy*. 2013: Springer Science & Business Media.
18. Chang H.-P., Sarkar T.K., and Pereira-Filho O.M., *Antenna pattern synthesis utilizing spherical Bessel functions*. IEEE Transactions on Antennas Propagation, 2000. **48**(6): pp. 853-859.
19. Shaw J.A., *Radiometry and the Friis transmission equation*. American journal of physics, 2013. **81**(1): pp. 33-37.
20. Yu A., Yang F., Elsherbeni A.Z., Huang J., and Rahmat-Samii Y., *Aperture efficiency analysis of reflectarray antennas*. Microwave Optical Technology Letters, 2010. **52**(2): pp. 364-372.
21. Gustafsson M. and Capek M., *Maximum gain, effective area, and directivity*. IEEE Transactions on Antennas Propagation, 2019. **67**(8): pp. 5282-5293.
22. Schmidt J.D. *Numerical simulation of optical wave propagation: With examples in MATLAB*. 2010. SPIE.
23. Voelz D.G., *Computational fourier optics: a MATLAB tutorial*. 2011: SPIE press Bellingham, Washington.
24. Jallod U.E. and Abood K.M. *Characteristics measurement of Baghdad University radio telescope for hydrogen emission line*. in *AIP Conference Proceedings*. 2019. AIP Publishing LLC.

محاكاة معاملات هوائي التلسكوب الراديوي الصغير عند التردد 1.42 غيغا هرتز

عدي عطوي جلود¹، حارث سعد مهدي¹، كمال محمد عبود¹
¹قسم الفلك والفضاء، كلية العلوم، جامعة بغداد، بغداد، العراق

الخلاصة

يقدم البحث نظرة عامة للسمات النظرية لمعاملات هوائي التلسكوب الراديوي الصغير. تتضمن المعاملات الأساسية عرض حزمة الهوائي، كسب الهوائي، كفاءة الفتحة ودرجة حرارة الهوائي. هذه المعاملات يجب ان تدرس بعناية لما لها من تأثير حاسم في الارصادات الفلكية الراديوية. محاكاة معاملات الهوائي نفذت لتقييم القابلية والكفاءة للتلسكوبات الراديوية الصغيرة لرصد مصدر نقطي عند تردد محدد. طبقت محاكاة عددية ثنائية الابعاد لفتحة دائرية منتظمة ولأنصاف اقطار مختلفة. ان قيم الأقطار اختيرت لتكون بين (1-10) م. ركزت هذه الدراسة على التلسكوب الراديوي الصغير ذو القطر 3 م، لكون هذا النوع من التلسكوبات شائع جداً في العالم. أظهرت نتائج هذه الدراسة ان نمط القدرة لهوائي قطره 3 متر يمتلك عرض حزمة بحدود 5 درجة. ايضاً تم حساب درجة حرارة الهوائي القصوى ووجدت انها بحدود أكثر من 3000 كلفن. هذه النتائج تتوافق بصورة جيدة مع بيانات رصدية حقيقية لخط الهيدروجين عند التردد 1.42 غيغا هرتز باستخدام التلسكوب الراديوي الصغير.